EXPERIMENTAL INVESTIGATION OF PERFORMANCE OF THE ROTORCRAFT DIRECTIONAL RUDDER

Andrej Novák[1,*], Karol Ścisłowski[2], Rafał Kliza[2], Robert Bąbel[3], Zbigniew Czyż[3], Paweł Karpiński[4]

[1]University of Zilina, Zilina, Slovakia
[2]Department of Thermodynamics, Fluid Mechanics and Aviation Propulsion Systems, Lublin University of Technology, Lublin, Poland
[3]Department of Airframe and Engine, Faculty of Aviation, Polish Air Force University in Deblin, Deblin, Poland
[4]Department of Machine Operation and Production Process Management, Faculty of Production Engineering, University of Life Sciences in Lublin, Lublin, Poland

*E-mail of corresponding author: andrej.novak@uniza.sk

Andrej Novak 0000-0002-9335-7206,
Rafał Kliza 0000-0002-7571-1582,
Zbigniew Czyż 0000-0003-2281-1149,
Karol Ścisłowski 0000-0003-0337-5863,
Robert Bąbel 0000-0002-9335-7206,
Paweł Karpiński 0000-0001-5786-1248

Resume

The paper presents the results of gyrocopter fuselage experiment testing in a wind tunnel. The model subjected to testing was made in 1:8 scale by 3D printing. The tests included the measurement of forces and aerodynamic moments acting on the model, for a variable fuselage sideslip angle β (-20º to 20º), and for three different positions of the rudder setting (0º, +5º, +10º). The measurement was carried out at an airspeed of 25 to 26 m/s. Based on the measured values, aerodynamic drag coefficients, lift coefficient and aerodynamic moment coefficients with respect to all axes of the reference system, were determined. The measurements carried out have facilitated the derivation of diverse characteristics, validating our conclusions. The results and conclusions drawn from these experiments can be valuable in enhancing the design and functionality of rotorcraft rudders.

Article info

Received 20 July 2023
Accepted 23 October 2023
Online 12 December 2023

Keywords:

gyrocopter
wind tunnel
aerodynamic research
directional rudder
sideslip angle

Available online: https://doi.org/10.26552/com.C.2024.007

ISSN 1335-4205 (print version)
ISSN 2585-7878 (online version)

1 Introduction

Aircraft designs, prior to flight testing, must be subjected to numerous simulation tests [1] and in wind tunnel [2-3]. In the case of studies conducted on pre-prepared test stands, even at the CAD (computer aided design) design stage, it is crucial to evaluate the adequacy of the applied design solutions in terms of reliability [4]. To enhance the safety of the conducted research, it is also worthwhile to continuously monitor the technical condition of the research setup, for example, by utilizing thermography [5]. As a result of these tests, the aerodynamic properties of the aircraft are determined, as well as the values of forces and moments acting on the structure [6]. It is also possible to determine the behavior of structures that may occur during flight [7]. Strength tests of fuselage covering samples [8] and computational simulations of the main rotor spar beams [9] are also being conducted to assess their load-carrying capacity during aerial operations. There are also solutions aimed at analyzing stresses in shape memory materials, which are also used in aviation [10]. This is crucial in terms of evaluating both the strength and the controllability and in-flight behavior of the structure. At the design stage, tests are conducted in a simulation environment. The development of computer programs has contributed to the use of advanced calculations of the means of transport design using the finite element method (FEM) [11]. The development of advanced simulation techniques has increased the popularity of simulation fluid dynamics in the form of CFD (computational fluid dynamics) simulations for the construction of unmanned aircraft prototypes [12-13] and aircraft propulsion systems [14]. Simulation studies of the lifting rotor [15-16] and the thrust propeller in the case of rotorcraft [17] also play a special role in rotorcraft

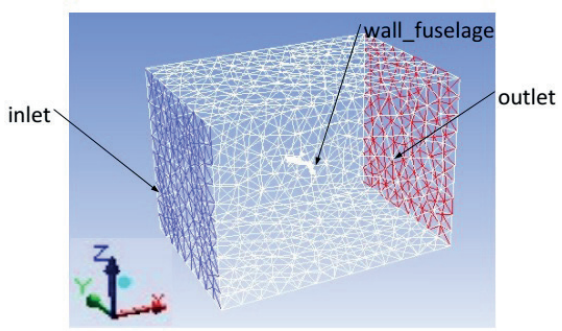

Figure 1 *Boundary conditions [25]*

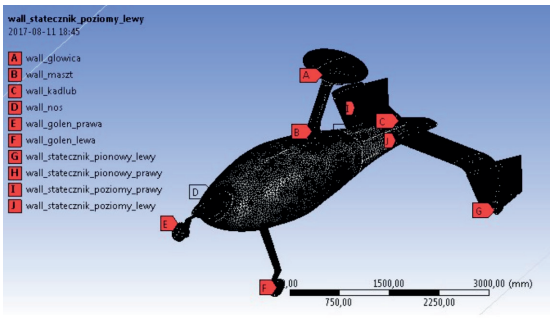

Figure 2 *Mesh of the gyrocopter model - isometric view [25]*

Table 1 *Parameters used in CFD simulation*

Parameter	Symbol	Value	Unit
Radius of the main rotor blade	R	5	m
Flight velocity	V	28	m/s
Air density	ρ	1.226	kg/m^3
Ambient temperature	T	288	K

design. Computer simulations are also used for research aimed at improving flight safety [18]. Once the physical prototype of the UAV (unmanned aerial vehicle) is built, the bench tests are conducted for the model, which is made at a reduced scale if necessary [19]. Tests conducted on the model allow for a significant reduction in the costs associated with making any changes to the design. In the case of an aircraft, one of the most common methods for conducting bench tests is tunnel testing. The wind tunnel allows determining the three-dimensional system of aerodynamic forces and moments acting on the model [20]. It is also possible to determine aerodynamic characteristics for different airflow velocities, varying angles of the model's orientation with respect to the airflow, or different configurations of the tailplane's orientation [21]. In recent times, one can see a trend toward the growing importance of unmanned aircraft [19], as well as ultralight aircraft [22] in the entire field of aviation. The wind-rotor, which is the subject of the described tunnel tests, is a very specific type of aircraft. It is a short takeoff and landing machine. The lifting force is generated by a lifting rotor, as in the case of helicopters, but it is put into rotary motion by the phenomenon of autorotation [23]. Control surfaces that operate similarly to aircraft are used to control altitude and direction. They are located on the tail boom, within the aerodynamic footprint of both the lifting rotor and the propeller, which means they must have relatively large surfaces [24].

2 Research object and methodology

2.1 The CFD calculations

Figure 1 shows that the research object's measurement zone takes the form of a cuboid with its sides positioned at a distance of 20 meters along the X-axis, 15 meters along the Y-axis, and 15 meters along the Z-axis, on both sides. The dimensions of gyrocopter are 6 348 mm in length, 2 802 mm in width, and 3 148 mm in height.

Within this specified computational domain, velocity inlet and pressure outlet conditions were defined. The other boundaries, which encompass the surfaces of the fuselage, have been designated as walls, but they are individually identified and referred to as integral components of the gyrocopter structure. These include the head, left leg, right leg, fuselage, mast, nose, left vertical stabilizer, right vertical stabilizer, left horizontal stabilizer, and right horizontal stabilizer.

To prepare the geometry of the gyrocopter for the CFD simulations, it was essential to make certain adjustments. Initially, the geometric model underwent refinement in CATIA v5, involving tasks such as connecting individual components, addressing specific deficiencies, discontinuities, and openings. Subsequently, the model was imported into the Ansys Workbench's Design Modeler. Here, further simplification occurred, primarily aimed at reducing the prevalence of fragmented surfaces, correcting any anomalies like acute angles, and smoothing out disjointed edges. Various tools were employed for these repair tasks, including Repair, Hard Edges, Edges, Sems, Holes, Silvers, Spikes, and Faces. Fragmented surfaces were fused together using the Merge tool. Following the necessary geometry simplifications, a fluid domain, or the research area, was created using the Enclosure tool. This step involved enclosing the research object within a cuboid. Figure 2 shows the created mesh of the research model of the gyrocopter.

This is the mesh created by the Tetrahedrons method with an advanced function of the curvature dimension. The inflation with the smooth transition

Table 2 *Technical data of the wind tunnel*

Description	Parameters
Measurement space diameter	1.05 m
Power of the driving motor	55 kW
Maximum air velocity	50 m/s
Working range: angles of attack	-35º to 35º
Sideslip angles	-20º to 20º

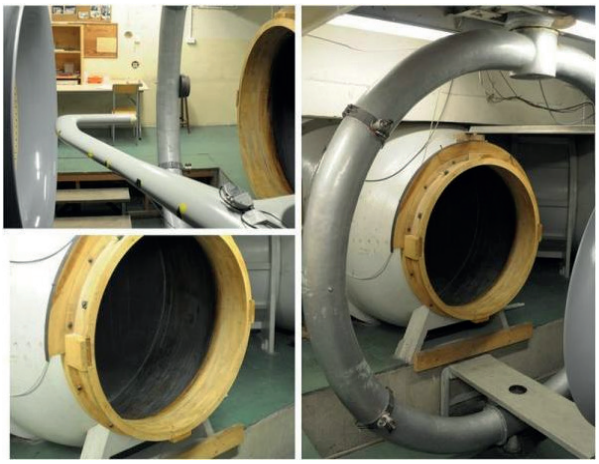

Figure 3 *The wind tunnel in which the study was conducted*

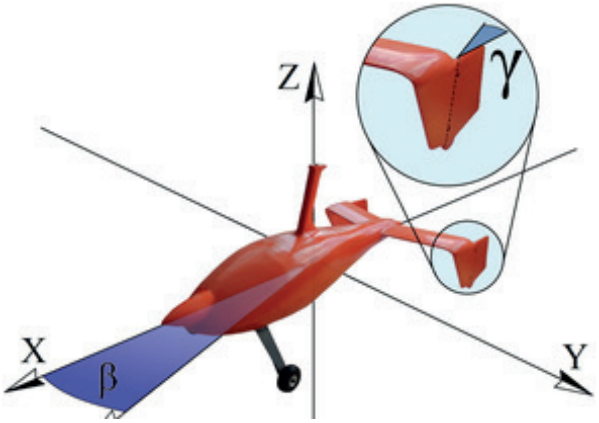

Figure 4 *Aduster gyrocopter model in 1:8 scale with variable angles β and γ*

with 7 layers and a growth rate of 1.15 was applied on the fuselage surface. The mesh was about 6.7 million cells in total. Table 1 presents the basic parameters used to perform CFD calculations [25].

2.2 Wind tunel

The research was carried out in a wind tunnel. The tunnel is used for weight measurements of aircraft models, airfoils or load-bearing airfoils. Its technical data are shown in Table 2.

The tunnel operates in closed air circulation. It has a wooden body and an open measuring space. The direction of air circulation is counterclockwise. The internal (stinger) and external (Witoshinsky scale) scales enable the weight measurements. Proprietary measurement software made in LabView allows automatic measurement and recording of the obtained results. Figure 3 shows the appearance of the wind tunnel.

Most often, the tunnel is used to conduct weight tests to determine aerodynamic characteristics. Both the whole structures and their components are tested.

2.3 Tested model

A model of the Aduster gyrocopter was tested. The solid model of the aircraft's fuselage was designed using the CATIA V5 software. The individual elements of the fuselage were made by 3D printing from PLA (polylactide) material. The model was made at a scale of 1:8. Figure 4 shows the appearance of the tested gyrocopter aircraft. Measurements were carried out for the fuselage model without the lifting rotor mounted.

Table 3 *Characteristic dimensions of the model [own development]*

Parameter	The actual gyrocopter	The model
r	5 m	0.625 m
$A = \varpi r^2$	78.5398 m^2	1.22718 m^2
$Ar = \varpi r^3$	392.699 m^3	0.766999 m^3

Figure 5 *Tested configuration with contraption, landing gear and nacelle*

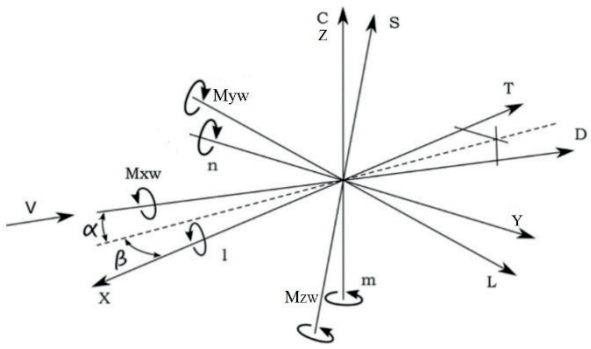

Figure 6 *The adopted coordinate system*

Table 3 shows a comparison of the dimensions of the actual aircraft with the made model.

2.4 Research methodology

The gyrocopter model was tested in several configurations and at different sideslip angles. For the purpose of this analysis, we considered the results obtained at an airspeed in the range of 25 to 26 m/s in the full configuration, i.e., with nacelle, landing gear, contrail, and a fixed fuselage angle of attack $\alpha = 0^{\circ}$.

The wind tunnel model of the gyrocopter was mounted on a measuring strain gauge scale. It was attached to the scale's boom by the rear tailplane, as shown in Figure 5. The measurement was carried out in the coordinate system associated with the model (body) F_b = [*T C N*], to move to the reference system associated with the velocity vector (wind) F_w = [*D S L*], rotation matrices by angle α and β were used according to Figure 6.

Figure 6 shows the direction of the velocity vector from which the system was deviated by an angle β. For all measurement points, the angle $\alpha = 0$. The local coordinate system of the model is the system [*x,y,z*] and the force system F_b is rotated about the *y* axis where the *C* axis and *y* axis are congruent. The local system of moments [*l,m,n*] is consistent with the [*x,y,z*] system.

Rotation matrices by angles α and β are:

$$R_\alpha = \begin{bmatrix} \cos\alpha & 0 & \sin\alpha \\ 0 & 1 & 0 \\ -\sin\alpha & 0 & \cos\alpha \end{bmatrix} \quad (1)$$

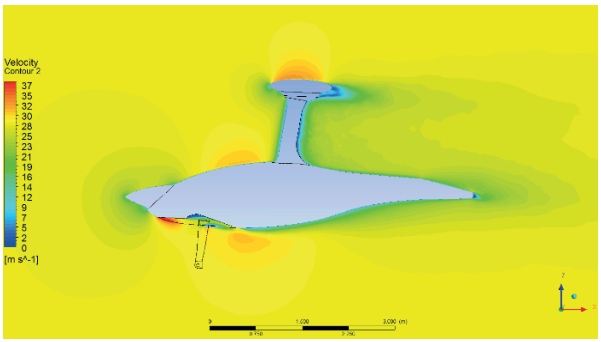

Figure 7 *Velocity distribution in the computational domain*

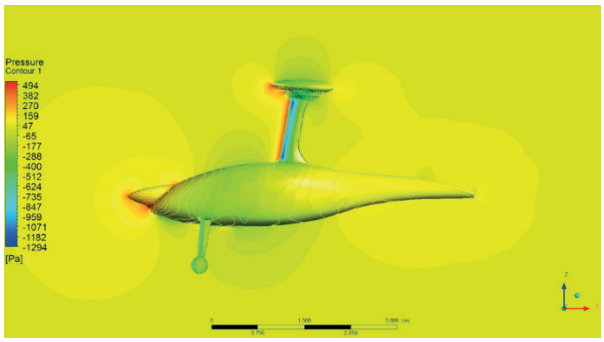

Figure 8 *Pressure distribution in the computational domain*

$$R_\beta = \begin{bmatrix} \cos\alpha & -\sin\beta & 0 \\ \sin\beta & \cos\beta & 0 \\ 0 & 0 & 1 \end{bmatrix} \tag{2}$$

Determining the force vector in the velocity vector system F_w, from the force vector in the model input F_b, requires the product:

$$F_W = R_\alpha R_\beta F_b\,. \tag{3}$$

The obtained matrix is binding in the rotation of the vector of moments. Force vectors in the coordinate system were determined. With respect to the set angles of attack and glide, the force vector takes the form:

$$\begin{bmatrix} D \\ S \\ L \end{bmatrix}(\alpha,\beta) = \begin{bmatrix} (T\cos\alpha + N\sin\alpha)\cos\beta - C\sin\beta \\ (T\cos\alpha + N\sin\alpha)\sin\beta - C\cos\beta \\ N\cos\alpha - T\sin\alpha \end{bmatrix}. \tag{4}$$

When determining the forces in the velocity system, the vector of moments takes the form:

$$\begin{bmatrix} Mx_w \\ My_w \\ Mz_w \end{bmatrix}(\alpha,\beta) = \begin{bmatrix} (l\cos\alpha + n\sin\alpha)\cos\beta - m\sin\beta \\ n\cos\alpha - l\sin\alpha \\ (l\cos\alpha + n\sin\alpha)\sin\beta + m\cos\beta \end{bmatrix}. \tag{5}$$

When changing the reference point from the point of the center of aerodynamic weight to the point of the center of gravity, relations occur:

$$F_2 = F_1\,, \tag{6}$$

$$M_2 = M_1 - r_{12}F_1\,, \tag{7}$$

$$\begin{bmatrix} l_2 \\ m_2 \\ n_2 \end{bmatrix} = \begin{bmatrix} l_1 \\ m_1 \\ n_1 \end{bmatrix} - \begin{bmatrix} 0 & -\Delta z & 0 \\ -\Delta z & 0 & \Delta x \\ 0 & \Delta x & 0 \end{bmatrix} \cdot \begin{bmatrix} T \\ S \\ N \end{bmatrix}, \tag{8}$$

where in the model used during the study:

$$\Delta x = 110\,mm\,, \tag{9}$$

$$\Delta z = 51\,mm\,. \tag{10}$$

Before each measurement series, a measurement of the reference signal *"tare"*, corresponding to signals in an aerodynamically unloaded system, was carried out. The measured values are subtracted from the measured signal.

3 Test results

3.1 The CFD results

Based on the CFD calculations carried out under the conditions described in section 2.1, air velocity and pressure distributions were obtained in the computational domain containing the gyrocopter model. The results were visualized on a plane symmetrically intersecting the model along the longitudinal axis. Calculations were carried out for measurement points including the variable: *sideslip angle* β in the range from -20° to 20°. The *angle of attack* α and the *rudder angle* γ were not variable and were 0° at all the measurement points of the CFD simulations. The numerical simulations generated numerical data containing the coefficients of forces and moments acting on the virtual gyrocopter model. Graphs of selected coefficients, determined by the numerical calculations, were compared to graphs representing the data acquired during the wind tunnel testing, presented in section 3.2. Figures 7 and 8 show the distribution of velocity and pressure in the computational domain for the measurement point α = 0°, β = 0°, respectively.

3.2 The tunnel results

The results were obtained in the form of measured values of forces and moments with respect to the three axes of the coordinate system. Measurements were made at a constant air velocity 25.5 (±0.5) m/s. For the conditions under which the measurements were carried out, the Reynolds number Re = $2.15{\cdot}10^6$ was determined. The measurements were made for three different configurations of the position of the γ-stay. Measurements were made in the neutral position, and with the directional rudder tilted by +5º and +10º. For each configuration the measurements were made for 13 different fuselage sideslip angles β (-20, -16, -12, -8,

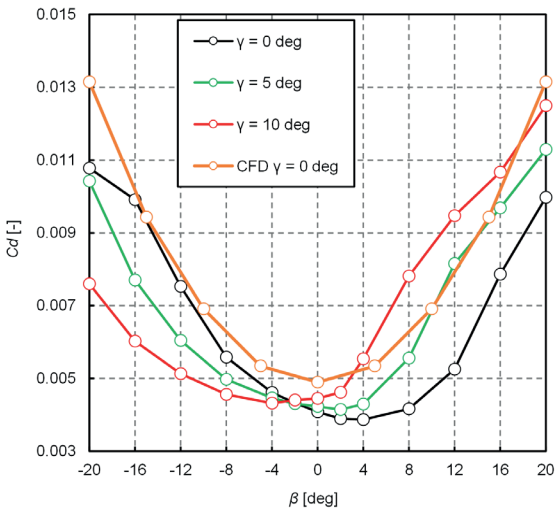

Figure 9 *Characteristics of aerodynamic drag coefficient C_d as a function of sideslip angle β*

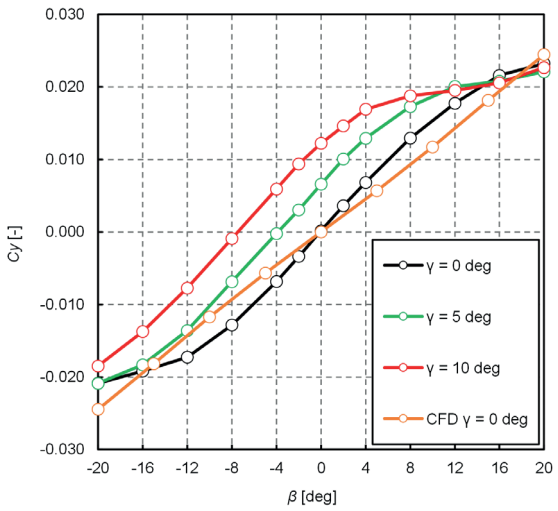

Figure 10 *Characteristics of the lateral force coefficient C_y as a function of fuselage sideslip angle β*

-4, -2, 0, 2, 4, 8, 12, 16, 20°). A total of 39 measurement points were taken.

Figure 9 shows the course of the aerodynamic drag coefficient of the fuselage, as a function of the fuselage sideslip angle β, for three different rudder deflections wedging height. The smallest aerodynamic drag coefficient was obtained at $\alpha = 4°$, when the rudder was set at $\gamma = 0°$. The coefficient of drag force was approximately $C_x = 0.004$. For the analyzed gyrocopter design, the deflection of the rudder in the range of 0 to 10°, with the fuselage positioned at an angle of $\beta = -2°$ does not significantly affect the value of the aerodynamic drag coefficient. The results obtained from the numerical simulations are represented by an orange line on the graph. The line is symmetrical about the vertical axis passing through the point $\beta = 0°$. The smallest drag force coefficient is $C_x = 0.005$ for $\alpha = 0°$. The simulation results of the drag force coefficient take values on average 25 % larger than the experimental results. This is due to differences between the physical model and the virtual model, which had an additional element on the mast to simulate the aerodynamic effect of the rotor. The additional surface caused the aerodynamic drag to increase.

Figure 10 shows the course of the lateral force coefficient as a function of the angle of lateral deflection of the fuselage. The results show that in the yaw range up to $\beta = 8°$, the lateral force is approximately linearly proportional to the angle of deflection of the directional rudder. Swinging the rudder in the direction of fuselage yaw, for angles $\beta > 12°$, does not significantly increase the lateral force. In the case of deflecting the directional rudder opposite to the direction of fuselage deflection, the limit of rudder effectiveness is reached at $\beta = -20°$. The course of the transverse force coefficient determined numerically intersects with the corresponding experimental course at $C_y = 0°$, $\beta = 0°$. The numerical characteristics in the whole range have a linear course. The results obtained during the tests show that after exceeding the value of the angle $\beta = \pm 12°$, the characteristics of the lateral force coefficient become nonlinear, and further increasing the inclination has less and less effect on further increasing the C_y coefficient. The characteristics of the effectiveness of the directional rudder is an important parameter in the design of automatic aircraft control systems and allows maximum effective use of aerodynamic properties.

An important parameter, when analyzing the performance of an aircraft's directional rudder is the torque coefficient with respect to the vertical axis (C_{mz}). The course of the obtained characteristics is shown in Figure 11. The shape of the vertical torque curves indicates a properly constructed rudder. The torque increment is proportional to the rudder deflection angle. At the same time, it is possible to indicate the angle $\beta = 16°$ as the limit of the effectiveness of the directional rudder, above which a change in the rudder angle will not affect the vertical aerodynamic moment of the gyrocopter. Simulations showed a smaller effect of fuselage angle on the value of lateral forces than during the wind tunnel tests.

In Figure 12, the characteristics of the lateral force coefficient C_y as a function of the drag force coefficient C_d is presented. From the polar plot below, it can be observed that an increase in the rudder deflection angle $\gamma = 5°$ and $\gamma = 10°$ does not significantly affect the change in C_d within the range of negative sideslip angles $\beta = -20°$, $\beta = -16°$. However, within the range of angles $\beta = -16°$, $\beta = 4°$, an influence of increasing rudder deflection angle γ can be seen on the increase in the lateral force coefficient C_z and the aerodynamic drag force C_d. Within the range of $\beta = 4°$, $\beta = 20°$, there is a sharp decline in the effectiveness of the rudder with an increase in the deflection angle γ. From the numerically calculated course of polar characteristics, it can be seen that the virtual model is affected by smaller

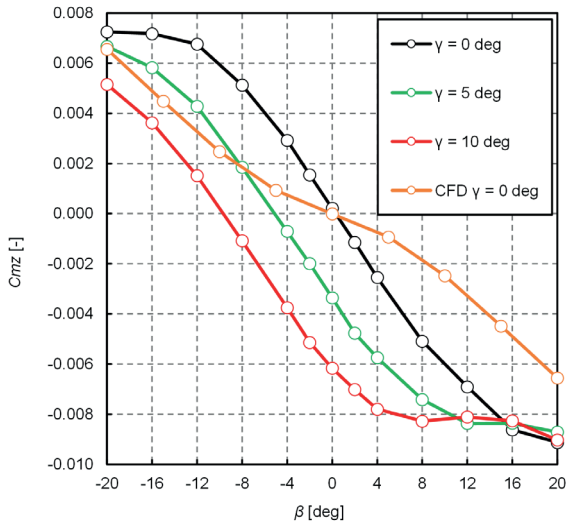

Figure 11 *Characteristics of the moment coefficient C_{mz} as a function of fuselage sideslip angle β*

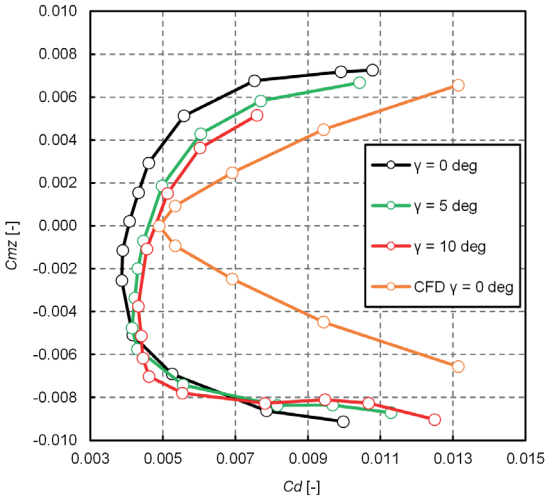

Figure 13 *The characteristics of the moment coefficient C_{mz} to drag force coefficient C_d*

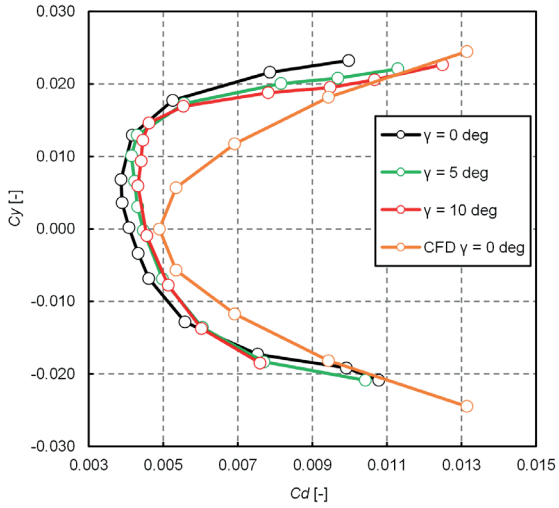

Figure 12 *The characteristics of the lateral force coefficient C_y as a function of drag force coefficient C_d*

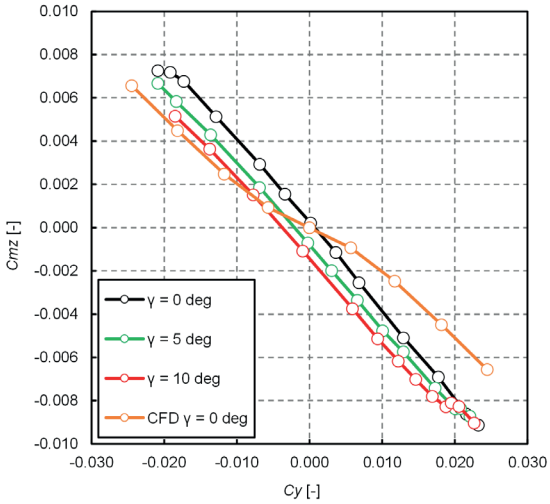

Figure 14 *The characteristics of the moment coefficient C_{mz} as a function of lateral force coefficient C_y*

lateral forces, which makes it less prone to drift. In the range of sideslip angles β from -15° + 15°, the side force coefficients C_z take values from -0.018 to 0.018. They are on average 50 the % lower than the values of C_z coefficients for experimental results.

Figure 13 presents a similar plot for the vertical moment coefficient C_{mz}. The resulting polar curves illustrate the relationship between the increase in the rudder deflection angle γ and the effectiveness of its operation, as determined by the value of C_{mz}. The black line shows the experimental results of the yaw moment coefficient value as a function of the aerodynamic drag force coefficient. The smallest value is 0.0045 for the yaw torque coefficient C_{mz} = -0.0025. The numerical simulation shows the smallest value of C_d = 0.005 corresponding to the torque coefficient C_{my} = 0. In the CFD simulation, increasing the angle β linearly affects the value of the torque coefficient C_{mz}.

Figure 14 presents the characteristics of the rotating moment coefficient C_{mz} as a function of the lateral force coefficient C_y. The graph illustrates how the lateral force coefficient varies with the aircraft sideslip angle. A clear difference can be seen between the experimental and simulation characteristics for a directional rudder angle γ = 0°. The moment curve of the simulation model intersects with the experimental curve at the point (0,0) of the adopted coordinate system. The simulation plot is characterized by a smaller than experimental C_{mz} coefficient by about 0.002 on average in the intervals β = (-20°, -5°) and β = (5°, 20°).

Figure 15 illustrates the characteristics providing information about the variation of the C_d/C_y ratio as a function of the sideslip angle of the fuselage. The curve's profile is consistent with theoretical assumptions. Depending on the angle β, forces along the Y-axis act in such a way that, at negative sideslip angles, the

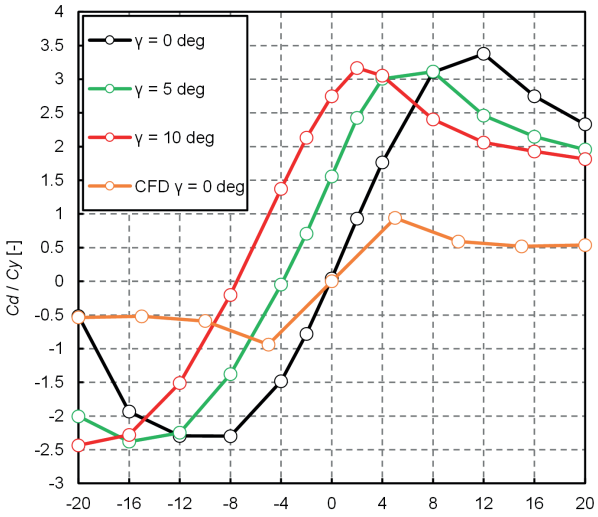

Figure 15 *The characteristics of the ratio of coefficients C_d/C_y as a function of the fuselage sideslip angle β*

fuselage operates in the opposite direction to the Y-axis. For positive values of the sideslip angle β, the aircraft operates in alignment with the Y-axis.

4 Conclusions

The construction of the full-scale aircraft is always a subject to certain discrepancies between the analytical aerodynamics calculations and the actual parameters of the fluid flowing around the aircraft. Therefore, it is necessary to conduct tests in a wind tunnel using a realistic model that replicates the aerodynamic parameters of the aircraft. Due to the high costs of creating a full-scale fuselage model, a favorable solution is to create a scaled-down replica to verify the accuracy of the analytical calculations and the behavior of the aircraft during the flight with less time, effort, and costs. A series of measurements conducted on the wind tunnel model of the aircraft allows for the analysis of the rudder's operation and its impact on flight mechanics. The conducted measurements have enabled the generation of various characteristics, based on which the following conclusions have been verified:

The variation of the drag coefficient C_d as a function of the sideslip angle has a parabolic shape. Depending on the set value of the sideslip angle β and the deflection angle of the rudder γ, the lowest values of the drag coefficient are within the range of -4° to 4°. The increase in the drag coefficient with the rudder deflection is related to the appearance of an additional surface area in the Y-Z plane on which the dynamic pressure acts. The shape of the characteristic for all the three rudder deflection angles γ is symmetrical with respect to the points of lowest C_d values and has a smooth profile, indicating that the measurement was conducted correctly.

The lateral force coefficient C_y as a function of the sideslip angle β, with zero deflection angle of the elevator $\gamma = 0$, has a linear trend within the range of -12° to 16°. In this range of angles, increasing the rudder deflection angle results in a proportional increase in the value of the lateral force coefficient C_y.

Deflecting the rudder by an angle γ results in a proportional increase in the yawing moment coefficient C_{mz} in the direction of the rudder deflection. This indicates that the rudder has been correctly designed.

The polar characteristics of the lateral force to drag force indicates that as the rudder deflection angle increases, the aerodynamic drag, represented by the C_d coefficient, increases as well.

From the characteristics in Figure 7, the effectiveness threshold of the rudder can be determined. It can be observed that for a sideslip angle of 16°, the rudder ceases to be effective.

The aerodynamic characteristics of the tested model exhibit profiles consistent with literature values. It can be concluded that the rudder in the presented aircraft fulfills its function properly.

The results of numerical simulations of the developed gyrocopter model differ from the experimental results. This is probably due to the additional component that simulated the aerodynamic drag of the rotor during CFD simulations. For the design reasons, the nacelle was not used in the tunnel tests.

Some discrepancies between the numerical and simulation results are due to the mounting of the tested model in the wind tunnel. The experimentally tested gyrocopter was fixed on the measuring scale with a beam that lowered the aerodynamic drag, which covered the rear of the fuselage, where under the normal conditions a vacuum is created that increases aerodynamic drag. For this reason, the aerodynamic drag coefficient for the CFD tests obtained a higher value than for the bench tests.

The study made it possible to assess the effect of

the sideslip angle γ on the aerodynamic properties of the entire aircraft fuselage, especially in the context of the relationship with the sideslip angle β. As a rule, a large value of sideslip angle results in a decrease in the lifting force generated on the lifting surfaces, an increase in the drag force and a change in the aerodynamic moment. An increase in the angle γ results in a decrease in the sideslip angle at which the minimum drag occurs. However, as expected, the minimum drag value corresponds to zero γ angle.

The conducted research allowed to formulate the following conclusions:

The sideslip force increases with an increase in the γ angle over the entire sideslip angle range. The value of the sideslip angle, corresponding to zero lateral force, decreases with an increase in the angle of the ballast. For a large value of γ angle (10°), the zero value of aerodynamic moment with respect to the Z-axis occurs at smaller values of sideslip angle. The developed C_y-C_d and C_{mz}-C_d polar characteristics allowed analysis of situations where there is a minimum aerodynamic drag and a maximum ratio of drag to side force or moment with respect to the Z - axis (yaw moment). This is important for analyzing the lateral stability of the aircraft and optimizing the geometry to minimize the drag.

The analysis carried out is important from the point of view of assessing the impact of the alignment of the applied contraption on the characteristics of the aircraft when performing maneuvers with a change in sideslip angle, i.e. when performing a turn. In a special case, there may be a simultaneous change in sideslip angle causing the aircraft to yaw with a simultaneous change in the aircraft's roll (a coordinated turn may then occur). The analysis carried out is a prelude to evaluation of the effect of the sideslip positioning on the characteristics of the aircraft during the execution of the turn maneuver.

The publication adds the results obtained from numerical tests. However, they differ to some extent from the results obtained from wind tunnel tests, as pointed out in the discussion. The probable reasons for the observed differences are also explained. The resulting data allows to illustrate the effect of flight conditions on the flight stability and behavior of the gyrocopter at different sideslip angles, and can also be used in flight control systems, such as fly by wire or autopilot systems. The paper adds the CFD simulation results that show the same configuration of the gyrocopter as in the wind tunnel tests. The results obtained can be used to better configure the simulation parameters, as well as provide knowledge on the behavior of the gyrocopter under certain flight conditions. Gyrocopters are a specific type of aircraft and their controls are different from those of airplanes and helicopters, so this type of data is very important.

Grants and funding

This work has been financed under Grant Agreement No. POIR.01.01.01-00-0056/16.

Conflicts of interest

The authors declare that they have no known competing financial interests or personal relationships that could have appeared to influence the work reported in this paper.

References

[1] HALE, L. E., PATIL, M., ROY, C. J. Aerodynamic parameter identification and uncertainty quantification for small unmanned aircraft. *Journal of Guidance, Control, and Dynamics* [online]. 2017, 40(3), p. 1-12. ISSN 0731-5090, eISSN 1533-3884. Available from: https://doi.org/10.2514/1.G000582

[2] CZYZ, Z., KARPINSKI, P., SKIBA, K., WENDEKER, M. Wind tunnel performance tests of the propellers with different pitch for the electric propulsion system. *Sensors* [online]. 2022, 22(1), 2. eISSN 1424-8220. Available from: https://doi.org/10.3390/s22010002

[3] TRAINELLI, L., ROLANDO, A. Reliable and cost-effective flight testing of ultralight aircraft. *Journal of Aircraft* [online]. 2011, 48(4), p. 1342-1350. eISSN 1533-3868. Available from: https://doi.org/10.2514/1.C031277

[4] SCISLOWSKI, K., SKIBA, K., WENDEKER, M., KLIZA, R., SIADKOWSKA, K., LUSIAK, T., NOVAK, A. Durability analysis of the prototype test rig for main rotors. *Communications - Scientific Letters of the University of Zilina* [online]. 2022, 24(2), p. B148-B157. ISSN 1335-4205, eISSN 2585-7878. Available from: https://doi.org/10.26552/COM.C.2022.2.B148-B157

[5] SIADKOWSKA, K., SCISLOWSKI, K., KLIZA, R., CZAJKA, B., WENDEKER, M. Thermal imaging monitoring of the prototype research installations. *AIP Conference Proceedings* [online]. 2021, 2429, 020036. ISSN 0094-243X, eISSN 1551-7616. Available from: https://doi.org/10.1063/5.0070428

[6] NEAL, D. A., GOOD, M. G., JOHNSTON, C. O., ROBERTSHAW, H. H., MASON, W. H., INMAN, D. J. Design and wind-tunnel analysis of a fully adaptive aircraft configuration In: 45th AIAA/ASME/ASCE/AHS/ASC Structures, Structural Dynamics and Materials Conference: proceeding [online]. 2004. eISBN 978-1-62410-079-6. Available from: https://doi.org/10.2514/6.2004-1727

[7] QUINTANA, A., VASCONCELLOS, R., THRONEBERRY, G., ABDELKEFI, A. Nonlinear analysis and bifurcation characteristics of whirl flutter in unmanned aerial systems. *Drones* [online]. 2021, 5(4), 122. eISSN 2504-446X. Available from: https://doi.org/10.3390/drones5040122

[8] SETLAK, L., KOWALIK, R., LUSIAK, T. Practical use of composite materials used in military aircraft. *Materials* [online]. 2021, 14(17), 4812. eISSN 1996-1944. Available from: https://doi.org/10.3390/ma14174812

[9] KLIZA, R., SCISLOWSKI, K., SIADKOWSKA, K., PADYJASEK, J., WENDEKER, M. Strength analysis of a prototype composite helicopter rotor blade spar. *Applied Computer Science* [online]. 2022, 18(1), p. 5-19. ISSN 2353-6977. Available from: https://doi.org/10.35784/acs-2022-1

[10] SCISLOWSKI, K., SIADKOWSKA, K. Comparative stress analysis of actuator models using smart material alloys. *AIP Conference Proceedings* [online]. 2021, 2429, 70663, ISSN 0094-243X, eISSN 1551-7616. Available from: https://doi.org/10.1063/5.0070663

[11] KOWALIK, R., KISILOWSKI, J., LUSIAK, T., GIL, L. Stability test of hyperloop vehicle in different movement conditions. *Eksploatacja i Niezawodnosc / Maintenance and Reliability* [online]. 2023, 25(3), 169204. ISSN 1507-2711, eISSN 2956-3860. Available from: https://doi.org/10.17531/ein/169204

[12] CZYZ, Z., KARPINSKI, P., SKIBA, K., SIADKOWSKA, K. Numerical analysis of the airflow around the gyro-one autogyro. *Journal of Physics: Conference Series* [online]. 2021, 1736(1), 012049. ISSN 1742-6596. Available from: https://doi.org/10.1088/1742-6596/1736/1/012049

[13] SZWEDZIAK, K., LUSIAK, T., GRZYWACZ, Z., DROZD, K. Numerical CFD analysis of an aerodynamic head cover of a rotorcraft motor. *Communications - Scientific Letters of the University of Zilina* [online]. 2018, 20(3), p. 42-47. ISSN 1335-4205, eISSN 2585-7878. Available from: https://doi.org/10.26552/com.c.2018.3.42-47

[14] JAKUBEK, D. Numerical simulation of temperature distribution in the gas turbine blade. *Communications - Scientific Letters of the University of Zilina* [online]. 2021, 23(3), p. B227-B236. ISSN 1335-4205, eISSN 2585-7878. Available from: https://doi.org/10.26552/COM.C.2021.3.B227-B236

[15] KROLAK, C., CZYZ, Z., SIADKOWSKA, K., KLIZA, R. CFD investigation of the main rotor for an unmanned helicopter. *Journal of Physics: Conference Series* [online]. 2021, 1736(1), 12054. ISSN 1742-6596. Available from: https://doi.org/10.1088/1742-6596/1736/1/012054

[16] RACZYNSKI, R., SIADKOWSKA, K., SCISLOWSKI, K., WENDEKER, M. An assessment of the transient effect on helicopter main rotor stability and power demand. *Combustion Engines* [online]. 2022, 191(4), p. 23-28. ISSN 2300-9896, eISSN 2658-1442. Available from: https://doi.org/10.19206/ce-146695

[17] KLIZA, R., WENDEKER, M., PYTKA, J., KASPRZAK, P. Simulation researches of the PROPWING airplane propulsion system. In: 2021 IEEE 8th International Workshop on Metrology for AeroSpace METROAEROSPACE: proceedings [online]. IEEE. 2021. eISBN 978-1-7281-7556-0, p. 698-704. Available from: https://doi.org/10.1109/MetroAeroSpace51421.2021.9511725

[18] KRASUSKI K., GOS, A. The numerical simulation of the atmosphere delays impact on radar measurement in aviation. *Communications - Scientific Letters of the University of Zilina* [online]. 2019, 21(4), p. 19-26. ISSN 1335-4205, eISSN 2585-7878. Available from: https://doi.org/10.26552/com.c.2019.4.19-26

[19] LING, W., DU, C., ZE, Y., XINDONG, N., SHUMAO, W. Research on the prediction model and its influencing factors of droplet deposition area in the wind tunnel environment based on UAV spraying. *IFAC-PapersOnLine* [online]. 2018, 51(17), p. 274-279. ISSN 2405-8971, eISSN 2405-8963. Available from: https://doi.org/10.1016/j.ifacol.2018.08.174

[20] LUSIAK, T., KORZEC, I., NOVAK, A., KOWALIK, R. Initial analysis of the aerodynamic characteristics of the rotorcraft model. *Transportation Research Procedia* [online]. 2022, 59, p. 203-213. ISSN 2352-1457, eISSN 2352-1465. Available from: https://doi.org/10.1016/j.trpro.2021.11.112

[21] BUSAN, R. C., MURPHY, P. C., HATKE, D. B., SIMMONS, B. M. Wind tunnel testing techniques for a tandem tilt-wing, distributed electric propulsion VTOL aircraft. In: AIAA Scitech 2021 Forum: proceedings [online]. 2021. p. 1-23. Available from: https://doi.org/10.2514/6.2021-1189

[22] BRDNIK, A. P., KAMNIK, R. Market and technological perspectives for the new generation of regional passenger aircraft. *Energies* [online]. 2019, 12(10), 1864. eISSN 1996-1073. Available from: https://doi.org/10.3390/en12101864

[23] SOMOV, Y. I., POLYNTSEV, O. Y. Nonlinear dynamics and robust control of a gyroplane rotor. In: 16th World Congress in Prague: proceedings. 2005.

[24] LUSIAK T., NOVAK A., JANOVEC M., BUGAJ M. Measuring and testing composite materials used in aircraft construction. *Key Engineering Materials* [online]. 2021, 904, p. 161-166. ISSN 1662-9795. Available from: https://doi.org/10.4028/www.scientific.net/KEM.904.161

[25] CZYZ, Z., KARPINSKI, P., LUSIAK, T., SZCZEPANIK, T. Numerical analysis of the influence of particular autogyro parts on the aerodynamic forces. *ITM Web of Conferences* [online]. 2017, 15, 07008. eISSN 2271-2097. Available from: https://doi.org/10.1051/itmconf/20171507008